

EIC Detector Simulations

E.C. Aschenauer, T. Burton, R. Darienzo and A. Kiselev

May 22, 2013

As part of its physics studies and detector development, the EIC task force has taken a two-pronged approach to detector simulation. The first is to perform detailed simulations, based on Geant in the FairRoot framework developed at GSI. This yields a realistic representation of the effects of detector performance, material budget, digitization and event reconstruction. The second is the use of a smearing generator developed within the group. This is based on simple parameterisations of detector resolution, and so provides less detail than full simulation, while being simpler to use and much faster to run. Here we provide a brief overview of the current status and capabilities of these tools.

For further details of EIC physics, please see the overview at:

https://wiki.bnl.gov/eic/index.php/DIS:_What_is_important

A summary of the kinematics of electron-hadron collisions and how these influence detector design can be found here:

https://wiki.bnl.gov/eic/index.php/DIS_Kinematics

The homepage for EIC Task Force Monte Carlo simulations is:

<https://wiki.bnl.gov/eic/index.php/Simulations>

1 EicRoot

1.1 Overview

EicRoot is a GEANT simulation package to be used for realistic EIC detector modelling. It is based on the FairRoot framework [1], adopted and maintained officially

at GSI (Darmstadt), and extensively uses PandaRoot codes developed for PANDA experiment [2]. Besides this it is linked against the **eic-smear** fast detector simulation package [3] which has been developed by eRHIC task force members over the last three years and is described in section 3.

Following FairRoot conventions, EicRoot detector geometries are prepared in either an ASCII format developed for the HADES experiment (tracking part) or as ROOT TGeo files (calorimeters).

Physics event lists are imported using library calls from the eic-smear package. So-called box generator usage for few-track configurations with predefined kinematics is also available. The possibility to switch between GEANT3 and GEANT4 transport engines is directly provided by the FairRoot framework.

Steering is done via ROOT C macros for simulation, digitization and reconstruction stages. Intermediate ROOT files are available for analysis and visualization after every stage. Output of the reconstruction stage is provided either as PandaRoot trees or in the eic-smear package format. It is technically possible to mix eic-smear functionality and full reconstruction (so that for instance charged particle momenta are given by realistic track fitting code while calorimeter energies are smeared by eic-smear code, for the same track).

The present EIC detector design includes a 3T solenoid with a significant transverse field component in the forward/backward tracker volumes at large rapidities. Solenoid modelling is in progress now (see section 2), and there exists an interface which allows usage of these simulated field maps in EicRoot framework.

Implementation of realistic beam pipe design, lepton and hadron beam line magnetic fields, as well as accommodation of beam optics for precise accounting of kinematic smearing and acceptance effects, are tasks for the near future.

Although a preliminary version of EicRoot package is installed on EIC computing cluster, at present it is still in the development stage. Tracking detectors and electromagnetic calorimetry are available in the geometry description already. Idealized reconstruction algorithms are implemented. These topics are covered in more detail in the following two subsections. Other parts of the setup (RICH, hadron calorimeters) are pending implementation.

1.2 Tracking detectors

Since the exact combination of tracking detectors used for the “final” version of the EIC setup is not decided at this point in time, the “simulation → digitization → reconstruction” sequence in EicRoot is designed in such a way that existing detectors can be easily turned on and off at any stage, and new detector templates can be added

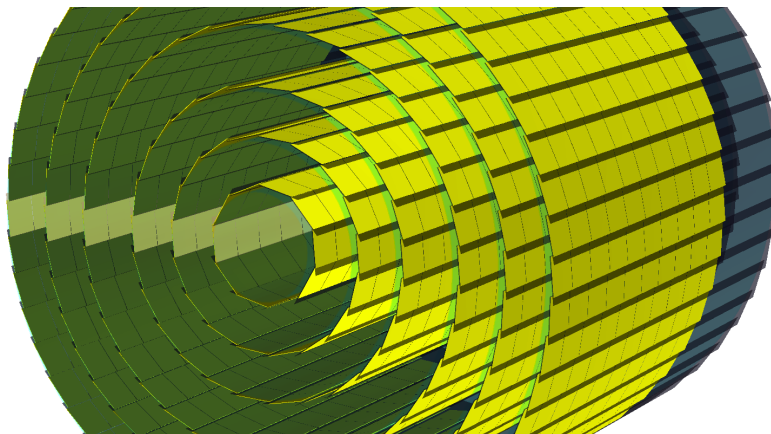


Figure 1: 3D cutaway view of the 6-layer MAPS pixel barrel silicon vertex tracker.

with minimal changes to the established reconstruction scheme. It is one of the main tasks of forthcoming physics simulations to optimize the setup and decide on the type and parameters of detectors.

A 6-layer barrel silicon vertex detector is implemented using thin MAPS pixel sensors [4] arranged in 10-chip “building blocks” which are presently under tests as part of a STAR tracker upgrade [5]. Geometry and cable assembly material distribution in the active acceptance is simulated precisely. A 3D cutaway view of this detector is shown in Fig. 1. Support structure details are not clear yet, so they are taken into account as cylindrical carbon fiber layers of appropriate thickness.

Forward and backward tracking detectors to register charged particles at large rapidities are composed of wedge-shaped silicon layers with the geometry following the layout of the ZEUS forward MVD [6]. The final design may however require usage of MAPS assemblies with smaller effective radiation length in the acceptance. A 3D view of the forward, backward and barrel silicon detectors is shown in Fig. 2.

A TPC filled with an $\text{Ar}/\text{CF}_4/\text{C}_4\text{H}_{10}$ gas mixture is the central tracking element of the setup. It has an effective length of 2 meters and an outer gas volume radius of 0.8 meters. Inner and outer field cages as well as the central membrane and the endcap frame are modelled as material layers of thickness matching the existing designs. It is assumed that readout will be realized via endcap GEMs with pad rows of 5 mm length in the radial direction, which will yield up to 100 space points per charged particle track. Cost/performance optimization of the readout pad geometry is one of the future simulation tasks. At present only an “ideal” digitization scheme is implemented, which accounts for the effects of electron cloud dispersion, but ignores subtle details of ionisation process, as well as possible signal overlap at the pad layer.

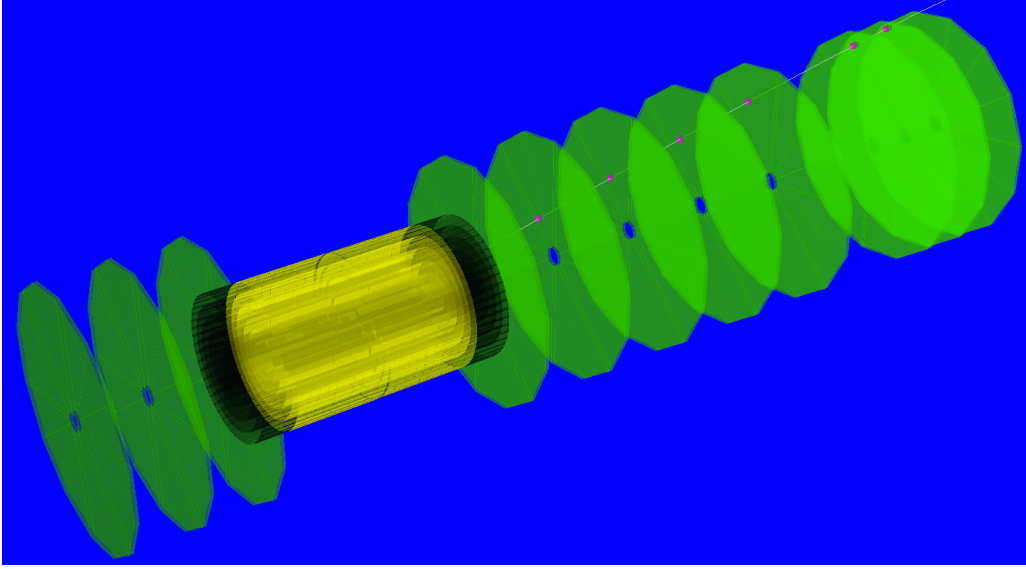


Figure 2: Forward, backward and barrel silicon trackers.

The present setup also includes a forward GEM tracker modelled after STAR FGT [7], which for now is used mainly as a detector template with reasonably high material budget and gaussian smearing of the measured coordinates.

So far only an ideal track “finder” is implemented, which assumes that charged particle hits do not merge together and their association with tracks is known *a priori*. This option is perfectly sufficient to model acceptance and perform track resolution studies. A simple, but more realistic approach to track finding, based on helix track search via a global Hough transform in parameter space, is in progress and first results are expected to come out soon. If this approach does not work well even at expected low EIC track multiplicities, more involved local track finding algorithms will become necessary.

The track fitting algorithm inherits a large amount of PandaRoot code based on GenFit [8] with Geane [9] track propagation, without any modifications. This demonstrates one of the clear advantages of using existing debugged software blocks available in the FairRoot environment. Fig. 3 shows the expected π^+ momentum resolution for the chosen combination of tracking detectors at different values of pseudo-rapidity. The simulation accounts material distribution and detector resolutions precisely; a Kalman filter algorithm [10] built into GenFit is used for optimal parameter estimates.

Work on the vertex code has not started yet. An approach based on the well-

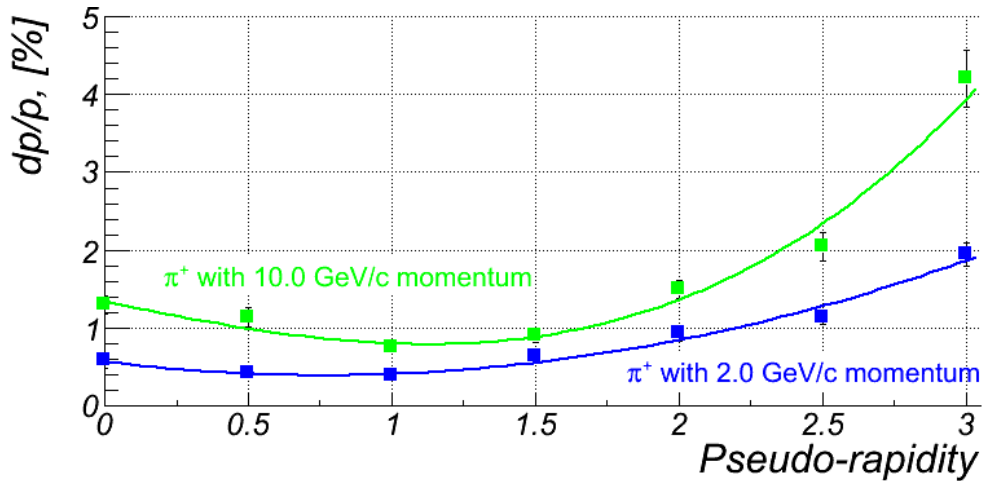


Figure 3: π^+ momentum resolution as a function of pseudorapidity for two different momentum values. The polynomial fits are intended only to guide the eye.

developed RAVE package [11], recently proposed for a STAR offline software upgrade [12], sounds promising here.

1.3 Electromagnetic calorimeters

This part of the EicRoot package uses basic FairRoot I/O and particle transport interfaces for simulation, but - contrary to the tracking detector implementation - does not employ any of the PandaRoot-specific codes for the reconstruction stage.

The implemented detectors are a PWO-crystal calorimeter in the backward direction and sampling tungsten powder scintillating fiber calorimeters in the forward direction and the barrel part.

Assuming the early stage of detector modelling, the geometry configurator for calorimeter layouts in EicRoot is specifically designed to be very flexible in terms of basic parameters, location, shapes and covered acceptance. Logical mapping tables are merged into the generated ROOT files with the GEANT geometry description. Therefore higher level software codes (digitization, clustering) do not contain any numbers, specifically hardcoded for a given selected geometry.

For the case of crystal calorimeter the configurator allows creation of both a “simple” geometry version, composed of rectangular crystal blocks covering the required acceptance in an almost gapless fashion, as well as a “projective rectilinear” geometry, which closely follows the layout of the PWO calorimeters of the CMS detector at CERN [13] and the future PANDA experiment at GSI [14]. In the latter option

tapered crystals are packed into groups, enclosed in carbon fiber alveoles and placed individually in order to provide the projective geometry configuration. Fig. 4 shows such a calorimeter hit by a simulated 10 GeV electron track. Detailed simulations should either confirm or discard the necessity of having the more complicated and expensive projective configuration in the final EIC detector setup.

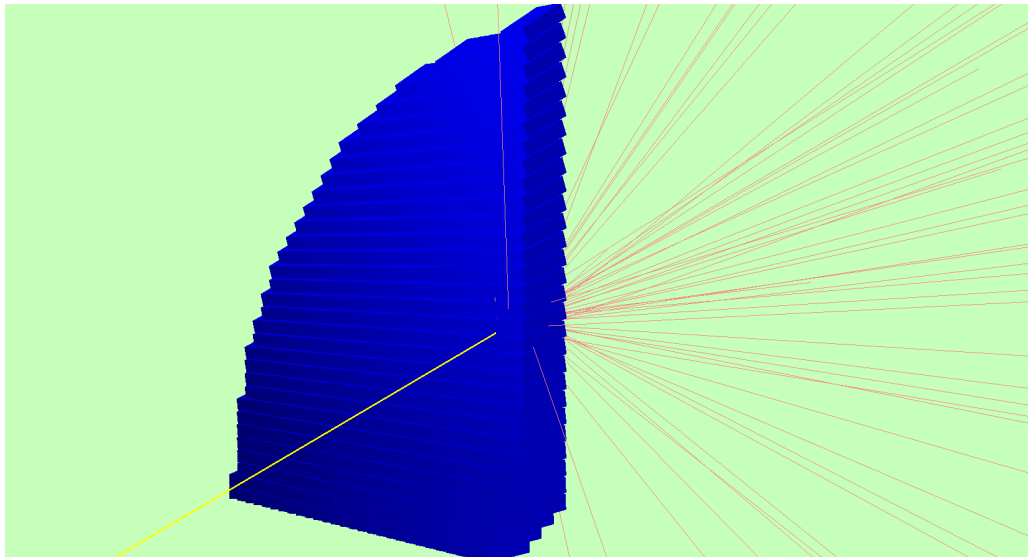
The forward sampling calorimeter assumes non-projective geometry. It is composed of “towers” which precisely describe the design presently under experimental tests [15]. The barrel non-projective sampling calorimeter is composed of the same “building blocks” as the forward one, except with a wedged shape in order to cover full the azimuthal acceptance without gaps. Both the “exact” geometry, with scintillating fibers as sensitive volumes, and the “smeared” one, with the tower material being a mixture of tungsten powder, epoxy and scintillators, can be created and passed through the complete software chain.

Only the “medium speed” simulation stage is implemented so far, which tracks electromagnetic showers up to the production of low energy e^+e^- pairs and records respective energy depositions in active material. The “fast” simulation code, which requires a reliable shower shape parameterization and produces integrated energy deposits based on particle energy and trajectory orientation with respect to the calorimeter matrix, is in progress. The “slow” version may be required later for the preshower modelling in order to simulate photon propagation in LYSO crystals and WLS material.

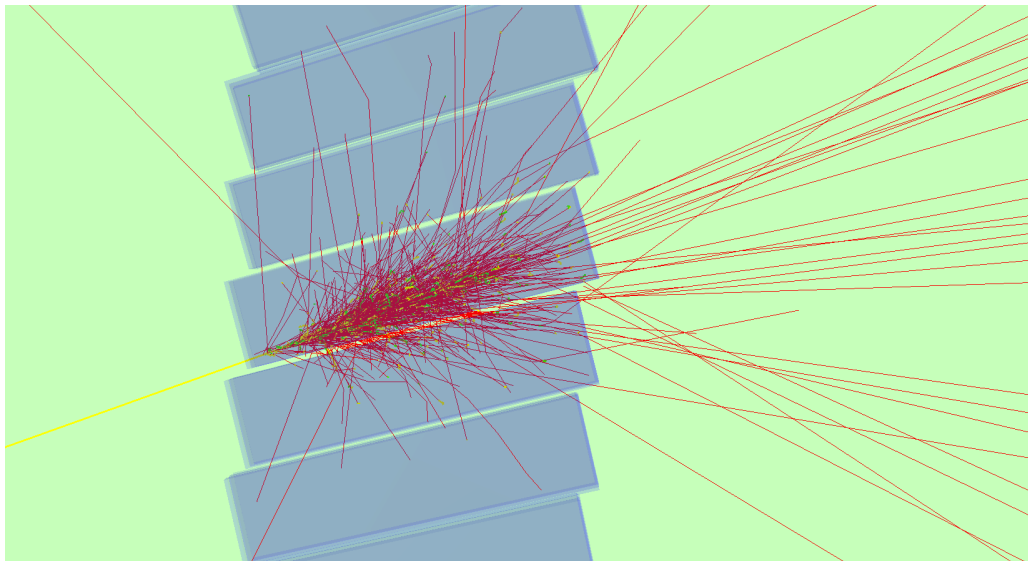
The digitization stage allows easy configuration of the necessary parameters (light yield, noise level, thresholds, attenuation length, decay times and timing gate, etc). As an option, a time plot with estimated photon arrival times to sensitive detectors can be generated and saved in the output ROOT file, as well as the plot showing estimated number of registered photons as a function of longitudinal track coordinate in the calorimeter.

Reconstruction code follows the logic of the ATLAS “topological clustering” algorithm [16] with configurable threshold parameters. Clusters can be directly associated with the GEANT primary mother particle which triggered them, for debugging purposes. A cluster splitting algorithm is not implemented so far, and should probably include tracking information from the very beginning.

Fig. 5 shows curves with the first simulated results for a forward sampling calorimeter on top of the experimental points measured in the T1018 test run. Further parameter tuning is clearly required; however, the simulation is already able to reproduce the measured values for this geometry reasonably well.



(a)



(b)

Figure 4: (a) A 3D view of the backward PWO electromagnetic calorimeter quadrant hit by a 10 GeV electron. The incoming electron track is highlighted in yellow. Photons leaking from the rear side are shown in pink. (b) Zoomed view of the same event with details of the electromagnetic shower development in the PWO crystals.

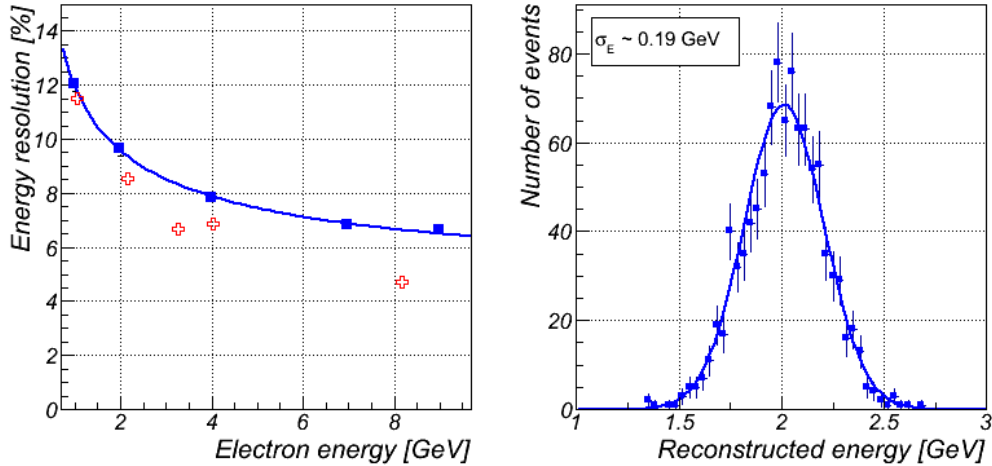


Figure 5: Left panel: energy resolution dependence of the backward fiber sampling electromagnetic calorimeter as a function of electron energy. Red crosses are measured data from Fig. 2.10 of [15]. Blue squares are simulation results obtained for this calorimeter geometry and a similar incident angle of electron beam with respect to the calorimeter tower axis. The fit is performed by a function $\sigma(E)/E = a+b/\sqrt{E}$. Right panel: fit results of the simulated data at 2 GeV beam energy.

1.4 Outlook

The following development path has been identified for EicRoot. Most tasks are envisaged to be complete by the end of this year. Further work on the tracking detectors will involve:

- Implementation of a realistic track finder.
- Addition of more detailed TPC digitization and tuning of pad geometry.
- Implementation of vertex code.

Further work on the calorimeters will involve:

- Optimization of the EMC simulation code.
- Implementation of a realistic clustering algorithm.
- Addition of hadronic calorimeters.
- Addition of a preshower detector to the backward EMC.

Other detector and interaction region elements to be developed are:

- Implementation of beam line elements and beam optics.
- Investigation of beam-induced background simulations.
- Optimization of magnetic fields.
- Investigation of a RICH implementation.

Other general items involve:

- Work on setup optimization (acceptance, resolutions, efficiency).
- Commencement of full physics simulations.
- Compilation of documentation.

2 Magnet Design

An important design goal for an EIC detector is to achieve good momentum resolution over a wide range in pseudorapidity. To this end, we have undertaken simulations of possible solenoid designs using the Opera magnetic simulation package. Our goal is to design a magnet that provides strong radial field in order to sufficiently bend particles with energies up to 10s of GeV and pseudorapidity up to approximately -5 so that their momentum can be determined with precision. Throughout the design process, we have been careful to avoid the dangers of high surface magnetic field. Although ample cooling of superconducting magnetic components may prevent quenches, we are wary of magnetic field strengths exceeding 6 T on the surfaces of any superconducting magnets. Beyond quenching fears, this practice also lends itself to overall cost concerns: the construction and operation of the magnet will be easier and cheaper if we utilize a lower and more uniform magnetic field.

Despite our best efforts at creatively thinking about how to maximize our momentum resolution, we havent yet gravitated away from a basic solenoid design, the MRS-B1. The MRS-B1 is a 2.4 m long magnet with an inner barrel radius of 1.0 m, made up of ten co-axial solenoids Fig. 6. Some rings have been highlighted for the convenience of the reader. The current field profile along the z-axis may be noted in Fig. 7. The MRS-B1 represents an attempt to optimize momentum resolution for particles in the forward region while still retaining experimental flexibility. Each rings current can be modified to change the field profile, allowing for magnetic fields as high as 3.0 T or as low as 0.5 T.

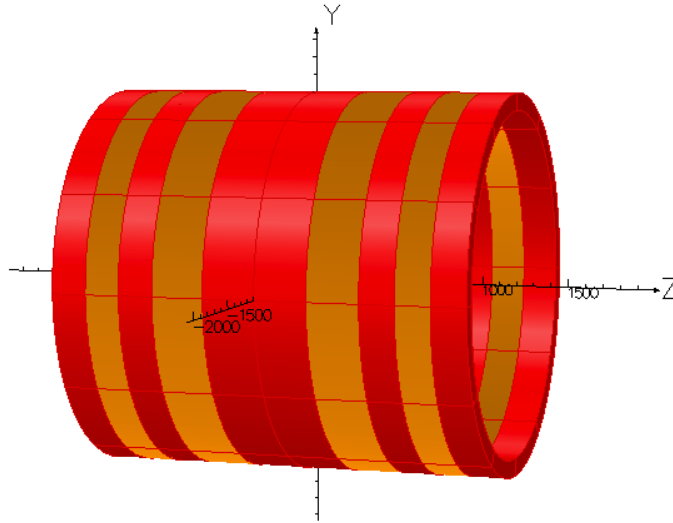


Figure 6: Segmented solenoid design, with rings carrying different currents.

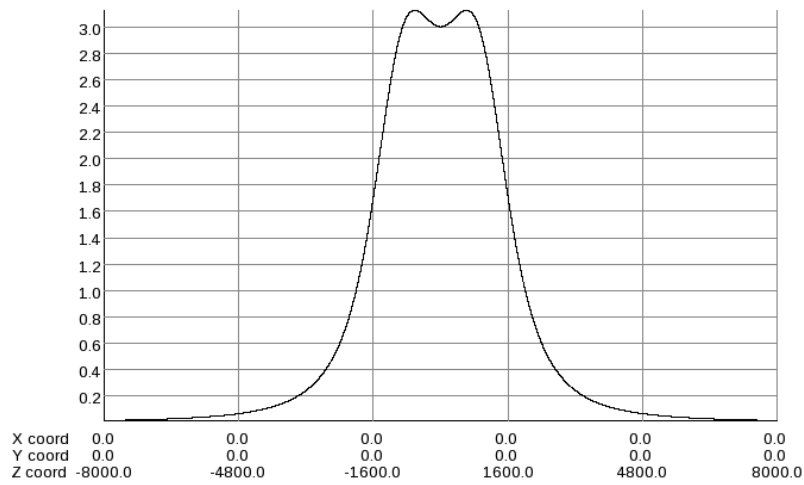


Figure 7: The resulting field profile along the z direction.

Particle energy	Initial angle in x-z plane	y location (mm)
5 GeV	2°	4.51 ± 0.01
	10°	23.18 ± 0.02
10 GeV	2°	2.26 ± 0.02
	10°	11.62 ± 0.02

Table 1: Electron trajectory simulations for magnet design MRS-B1 showing the location of electrons along the y axis at $z = 1,200$ mm. Electrons are initially emitted in the x-z plane, so movement in the y direction is due solely to bending in the magnetic field.

The barrel field and radius have not yet been optimized for the placement of a TPC. Current TPC simulations require field uniformity over a length in z of 2.0 m. The addition of an iron yoke for shielding and flux return will allow us to use lower current densities in each ring. An iron yoke may even allow us to exclude some rings in favor of iron substitutes, which would greatly increase radial field components within the barrel region. The addition of a yoke is also very important for equipment and personnel shielding. Currently, magnetic fields outside of the magnet barrel (x and y axes) are around 0.2 T and over 1.0 T in the forward z-region. Particle simulations in OPERA 3D yield the results in table 1. The electron locations are listed at the end of the magnet, where the end cap detector would likely begin.

Utilizing the magnets symmetry, we can construct 2D models of the magnet using only half of the barrel in OPERA 2D. This allows us to unambiguously see magnetic field (potential) lines for the MRS-B1 (Fig. 8).

3 Smearing Package

The **eic-smear** package provides a means for applying detector smearing to Monte Carlo (MC) data, whereby kinematic properties from the MC particles are modified according to a description of detector performance (both acceptance and resolution). The package contains a series of classes and functions to facilitate the smearing of ROOT trees created from Monte Carlo. The functionality to generate these input trees is also included in the eic-smear package. It is intended to be extremely flexible, allowing users to change detector properties quickly and painlessly.

Smearing is designed to allow rapid, albeit approximate, estimates of the effect of detector performance on physics observables. As implemented in eic-smear, it is

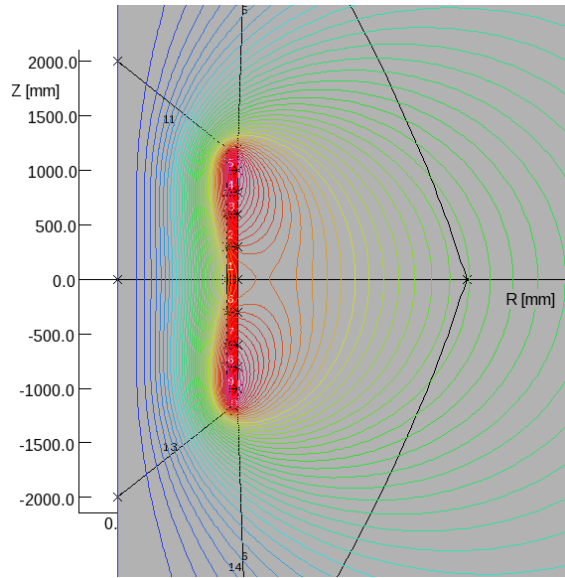


Figure 8: Magnetic field lines in a cross section through the MRS-B1 solenoid. The material of the solenoid is shown by the red rectangle.

much faster to run than a full detector simulation (e.g. Geant), both in terms of user time spent specifying the detector properties and in CPU time spent processing events. For example, the smearing code typically processes hundreds to thousands of events per second on a modern CPU, which is comparable to the generation rate of many of the event generators supported natively in the package. Compare this to the performance of a detailed Geant simulation, where specifying the detector properties with sufficient realism can be very time-consuming, and events may each take many seconds to be processed. That said, the smearing code is *not* intended as a replacement for full detector simulations. Rather, it is a complimentary tool for assessing the impact of changes in detector performance on a physics measurement, in a way that is much more rapid, but less detailed, than a full detector simulation. The smearing code is also designed to be easily extensible by users, by adding new classes inheriting from those included with the package.

The website [3] contains more detailed documentation on the contents and use of the package, and links to detailed code documentation for those wishing to extend the code themselves.

Subsystem	Acceptance	$\sigma(x)$
Electromagnetic calorimeter	$-2 < \eta < 2$	$12.2\% * \sqrt{E}$
	$-4.5 < \eta < -2$	$1.78\% * \sqrt{E} + 0.69\% * E$
Hadronic calorimeter	$1 < \eta < 4.5$	$38\% * \sqrt{E}$
Tracking	$-1 < \eta < 1$	$0.1\% * p$
	$-2 < \eta < 1, 1 < \eta < 3$	$1\% * p$
	$-4.5 < \eta < -2$	$5\% * p$
PID for π, K, p	$-3 < \eta < 3$	HERMES matrix
PID for e^\pm, γ	$-4.5 < \eta < 4.5$	Perfect

Table 2: Parameters describing a simple “baseline” EIC detector performance. Particle identification (PID) for electrons and photons is assumed to be perfect over the entire acceptance. Angular smearing is neglected, being assumed to be small compared to momentum resolution.

3.1 Example Results

To demonstrate the utility of eic-smear, we consider a simple “baseline” detector performance implemented in the smearing framework, as summarised in table 2. Figure 9 shows the resolution for some basic particle properties, from simulation of 20 x 250 GeV electron-proton events in PYTHIA 6.4.

As an example of using eic-smear in more complicated studies, we consider reconstruction of event kinematics using the hadronic final state. In a normal DIS event, kinematics quantities such as x and Q^2 are calculated from the properties of the scattered beam electron. In a charged-current interaction, the electron is converted into a neutrino and is thus unmeasured. Kinematics must therefore be reconstructed from what *is* measurable, namely the final state products of the breakup of the beam proton. Precise reconstruction of the event kinematics is essential to the precision physics of an EIC.

Investigating the effect of detector performance on such a measurement is a complicated task; it does not depend simply on a single quantity, but on the sum of momenta and energies of all measurable particles. It is thus affected by both detector acceptance (which particles are measured) and resolution (how well they are measured). Performing a full detector simulation for this purpose, while desirable in the long term, is far from trivial; it requires detailed descriptions of each component to be implemented in Geant. Furthermore, at present the EIC detector is in the R&D stage, thus many questions remain open about exactly *what* technol-

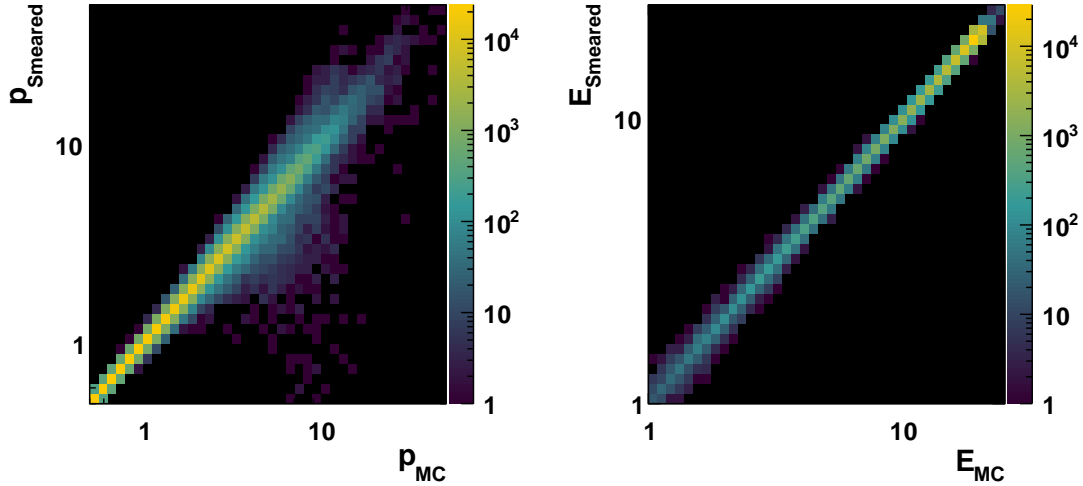
(a) π^\pm momentum resolution(b) Scattered e^\pm energy resolution

Figure 9: Resolution in a charged pion momentum and scatted electron energy.

ogy choices will be made. Fully implementing a large number of different options in Geant is prohibitively time-consuming. Thus, this problem is ideally suited to a smearing approach. The utility is twofold; firstly, an approximate detector performance can be implemented to see the impact on kinematic reconstruction. Secondly, a variety of different performances can be investigated (without reference to any specific technology) to provide minimum requirements as guidance to those developing detectors.

Figure 10 shows the result of such a study into the Q^2 and x resolution of an EIC detector, using charged-current events from the DJANGO event generator with 20×250 GeV electron-proton collisions. The correspondence between the true values and those reconstructed by the detector, accounting for its acceptance and performance, is good. This shows both what is achievable with a given detector performance, and gives guidance for performance requirements to detector designers. In the smearing framework, the specifics of the detector acceptance and resolution can be rapidly modified to investigate their effects on kinematic resolution.

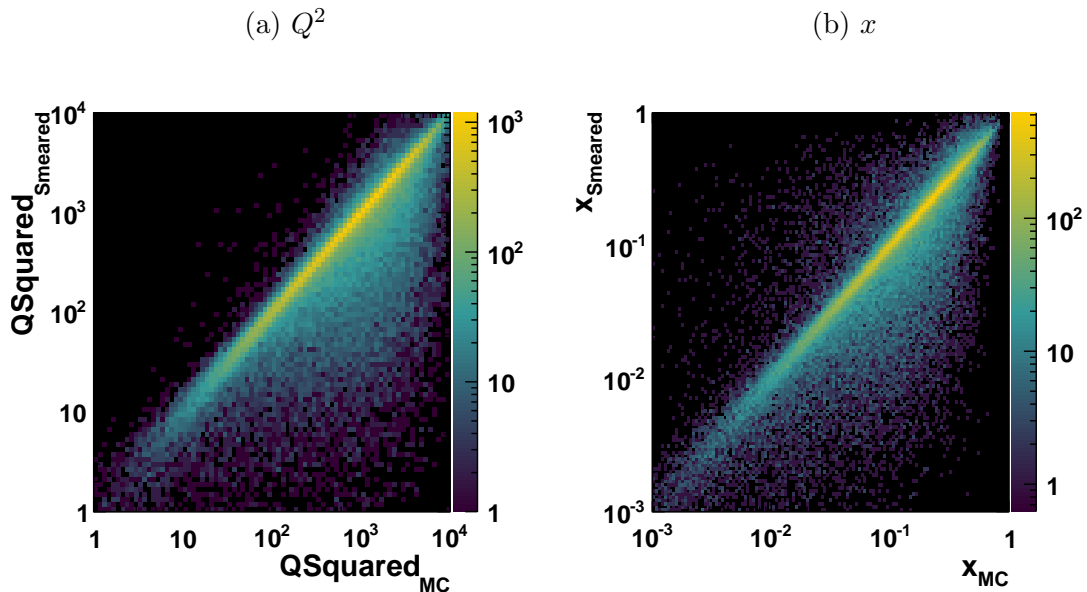


Figure 10: Q^2 resolution via the Jacquet-Blondel method with an assumed “baseline” EIC detector performance.

3.2 Outlook

The core features that were initially envisaged for eic-smear have now been implemented. The code now runs stably, and has a significant amount of documentation to guide new users. Output from eight Monte Carlo generators used in the EIC task force can be processed; support for further generators will be added if and when they become needed.

Detailed studies are planned into hadronic and mixed electron-hadron methods for calculating kinematics, expanding on the study summarised in section 3.1. In the medium term, additional functionality allowing vertex smearing will be added. This will be important in, for example, studies of charm mesons.

A Example eic-smear ROOT script

Below is an example of a ROOT script for constructing a very simple detector description. Please see the documentation on the website for details of the meaning of the classes involved.

```
Smear::Detector BuildExample() {
    // Create an electromagnetic calorimeter with
    // sigma(E) = 20% * sqrt(E)
    // Genre == 1 (third argument) means only
    // photons and electrons are smeared
    Smear::Device emcal(Smear::kE, "0.2*sqrt(E)", 1);
    // Create our tracking capabilities, by a combination
    // of momentum, theta and phi Devices.
    Smear::Device momentum(Smear::kP, "0.01 * P");
    Smear::Device theta(Smear::kTheta, "0.05 * P");
    // "0" indicates perfect performance i.e. sigma(phi) = 0
    Smear::Device phi(Smear::kPhi, "0");
    // Create a based on Hermes RICH.
    Smear::ParticleID rich("PIDMatrix.dat");
    // Our detector only covers the central region
    Smear::Acceptance::Zone central(TMATH::Pi() / 4.,
                                    3. * TMATH::Pi() / 4.);

    emcal.Accept.AddZone(central);
    momentum.Accept.AddZone(central);
    theta.Accept.AddZone(central);
    phi.Accept.AddZone(central);
    rich.Accept.AddZone(central);
    // Create a detector and add the devices
    Smear::Detector det;
    det.AddDevice(emcal);
    det.AddDevice(momentum);
    det.AddDevice(theta);
    det.AddDevice(phi);
    det.AddDevice(rich);
    // The detector will calculate event kinematics from smeared values
    det.SetEventKinematicsCalculator("NM JB DA");
    return det;
}
```

References

- [1] M. Al-Turany et al, J. Phys. Conf. Ser. 396 (2012) 022001
- [2] S. Spataro (for the PANDA Collaboration), J. Phys. Conf. Ser. 331 (2011) 032031
- [3] <https://wiki.bnl.gov/eic/index.php/Eic-smear>
- [4] <http://www.iphc.cnrs.fr/List-of-MIMOSA-chips.html>
- [5] See eg. L. Greiner, LBNL instrumentation seminar 08/29/2012
- [6] E. Koffeman, Nucl. Instr. Meth. A453 (2000) 89
- [7] F. Simon et al, arXiv: 0811.2432v1
- [8] C. Hoepfner et al, Nucl. Instr. Meth. 620 (2010) 518
- [9] V. Innocente, M. Maire and E. Nagy, GEANE CERN Writeup, July 1991
- [10] R. Fruehwirth, Nucl. Instr. Meth. A262 (1987) 444
- [11] W. Waltenberger et al, J. Phys. Conf. Ser. 119 (2008) 032037
- [12] D. Arkhipkin and Y. Zulkarneeva, STAR tracking review meeting 04/16/2013
- [13] G. Bayatian et al, CMS TDR 4, CERN/LHCC 9733 (1997)
- [14] W. Erni et al, arXiv: 0810.1216v1 (2008)
- [15] The EIC Calorimeter R&D Consortium, Nov. 2012 Renewal Proposal for RD2012-14
- [16] W. Lampl et al, ATL-LARG-PUB-2008-002 (2008)